Masteroppgave

NTNU
Norges teknisk-naturvitenskapelige universitet

Nils Marius Kvam Sakserud

Centrifugal Pump For a Rocket Engine

Trondheim, Jul. 2019

Masteroppgave i
Januar

NTNU
Kunnskap for en bedre verden

NTNU
Norges teknisk-naturvitenskapelige universitet
Institutt for energi- og prosessteknikk

EPT-M-2019-

MASTEROPPGAVE

for

Student Johannes Nils Marius Sakserud

Våren 2019

Design av en sentrifugalpumpe for en rakett
Design of a centrifugal pump for a rocket

Bakgrunn

I det 20. århundre var verdensrommet kun tilgjengelig for et fåtall nasjoner, finansiert av skatter og realisert av offentlige institusjoner. Det siste tiåret har investering i og utvikling av ikke-statlige romprogram skutt fart. Svært mange aspekter av våre liv i dag muliggjort av satellitteknologi, og hundretalls nyetablerte selskap jobber med innovative måter å bruke rommet på. Vi har kommet til en tid der utviklingen vil skyte enda høyere fart. Mindre orbitale raketter kan bli skutt opp til langt lavere pris enn tidligere antatt. Det som omtales som den nye romalderen, omhandler demokratisering og kommersialisering av verdensrommet.

Den raske utviklingen i batterier og elektriske motorer de siste årene, har ført oss til punktet hvor elektriske pumper i bæreraketter er muliggjort. En elektrisk turbopumpe er mer fleksibel i bruk, rimeligere og langt tryggere. For kunden gir dette lavere risiko, kortere utviklingstid og lavere utviklingskostnader, noe som gjør dette en mer attraktiv løsning for unge selskaper og mindre bæreraketter.

Mens turbinbaserte pumper er tett knyttet til motoren de skal drive, og må designes fra bunnen for hver enkelt motor, kan elektriske turbopumper lettere designes parametrisk. Det medfører en stor fordel, da man i større grad kan bruke ett enkelt design og tilpasse det ulike rakettmotorer. De eneste relevante parameterne som endrer seg mellom ulike motorer er ønsket trykk, ønsket gjennomstrømning og drivstoffets tetthet. I denne oppgaven vil det fokuseres på prosessen med å ta nevnte parametere for å gjennomføre et komplett design for en spesifikk motor.

Mål

Gjennomføre hydraulisk design av en sentrifugalpumpe som skal benyttes i en rakett

Oppgaven bearbeides ut fra følgende punkter:

1. Litteraturstudie av relevante sentrifugalpumpe design
2. Software
    a. DAK-program: Creo
    b. CFD-program; CFX - ANSYS
    c. Matlab eller Pyton
3. Design av sentrifugalpumpens innløp, løpehjul, diffusor og spiraltromme basert på empiri
4. 3D-DAK tegning av hele pumpen
5. CFD-analyse
    a. Løpehjul
    b. Komplett pumpe med innløp, løpehjul, diffusor og spiraltromme

Senest 14 dager etter utlevering av oppgaven skal kandidaten levere/sende instituttet en detaljert fremdrift- og eventuelt forsøksplan for oppgaven til evaluering og eventuelt diskusjon med faglig ansvarlig/veiledere. Detaljer ved eventuell utførelse av dataprogrammer skal avtales nærmere i samråd med faglig ansvarlig.

Besvarelsen redigeres mest mulig som en forskningsrapport med et sammendrag både på norsk og engelsk, konklusjon, litteraturliste, innholdsfortegnelse etc. Ved utarbeidelsen av teksten skal kandidaten legge vekt på å gjøre teksten oversiktlig og velskrevet. Med henblikk på lesning av besvarelsen er det viktig at de nødvendige henvisninger for korresponderende steder i tekst, tabeller og figurer anføres på begge steder. Ved bedømmelsen legges det stor vekt på at resultatene er grundig bearbeidet, at de oppstilles tabellarisk og/eller grafisk på en oversiktlig måte, og at de er diskutert utførlig.

Alle benyttede kilder, også muntlige opplysninger, skal oppgis på fullstendig måte. For tidsskrifter og bøker oppgis forfatter, tittel, årgang, sidetall og eventuelt figurnummer.

Det forutsettes at kandidaten tar initiativ til og holder nødvendig kontakt med faglærer og veileder(e). Kandidaten skal rette seg etter de reglementer og retningslinjer som gjelder ved alle (andre) fagmiljøer som kandidaten har kontakt med gjennom sin utførelse av oppgaven, samt etter eventuelle pålegg fra Institutt for energi- og prosessteknikk.

Risikovurdering av kandidatens arbeid skal gjennomføres i henhold til instituttets prosedyrer. Risikovurderingen skal dokumenteres og inngå som del av besvarelsen. Hendelser relatert til kandidatens arbeid med uheldig innvirkning på helse, miljø eller sikkerhet, skal dokumenteres og inngå som en del av besvarelsen. Hvis dokumentasjonen på risikovurderingen utgjør veldig mange sider, leveres den fulle versjonen elektronisk til veileder og et utdrag inkluderes i besvarelsen.

I henhold til ”Utfyllende regler til studieforskriften for teknologistudiet/sivilingeniørstudiet” ved NTNU § 20, forbeholder instituttet seg retten til å benytte alle resultater og data til undervisnings- og forskningsformål, samt til fremtidige publikasjoner.

Besvarelsen leveres digitalt i DAIM. Et faglig sammendrag med oppgavens tittel, kandidatens navn, veileders navn, årstall, instituttnavn, og NTNUs logo og navn, leveres til instituttet som en separat pdf-fil. Etter avtale leveres besvarelse og evt. annet materiale til veileder i digitalt format.

☐ Arbeid i Vannkraftlaboratoriet
☐ Feltarbeid

NTNU, Institutt for energi- og prosessteknikk, 14. januar 2019

_____
Ole Gunnar Dahlhaug
Faglig ansvarlig/veileder

Medveiledere:

- Eivind Liland
- Chirag Trivedi

1 Preface

This Master's thesis has been written at the Waterpower laboratory at the Norwegian University of Science and Technology by Nils Marius Kvam Sakserud during the spring of 2019

My work throughout the semester has solely consisted of trial and error in centrifugal pump design. The learning curve has been steep, and I am very grateful for the opportunity to carry out this project.

I would like to thank my supervisor Ole Gunnar Dalhaug for the interesting discussions throughout the semester, and how he has lead me through this project with his supportive and positive attitude. I would also like to thank my co-supervisor Eivind Liland from Orbital Machines for giving me the opportunity this opportunity.

Lastly, I would like to thank my family, especially my sister, who has been very supportive the last weeks.

Nils Marius Kvam Sakserud
07.07.2019

2 Abstract

The objective for this Master's thesis was to design and perform CFD analysis of centrifugal pump for a rocket engine. Besides delivering the required pressure, zero cavitation was set as a requirement for a successful design. Numerous designs and simulations where carried out. The final impeller design fulfilled the requirement of both the pressure rise of 40 bar, while still avoiding cavitation. As the simulation of the pump in its entirety did not reach a satisfying convergence criteria, the volute losses are still uncertain. Hence, the outlet pressure of the pump is not yet determined.

3 Sammendrag

Oppgaven i denne masteroppgaven var å designe og gjennomføre numerisk strømningsberegning på en sentrifugalpump ment for en rakettmotor. Pumpen skulle, i tillegg til å levere ønsket trykkøkning, kjøre totalt uten kavitasjon. Flertallige design og simuleringer ble gjennomført. Resultatene fra den siste impellersimuleringen viste lovende resultater både med tanke på ønsket trykkøkning, samt kavitasjonsegenskaper. Simuleringen av pumpen i sin helhet nådde ikke tilfredstillende krav i forhold til konvergenskriteriene som ble satt, og tapene i spiraltrommen er derfor uvisst. Derfor er ikke trykket ved pumpens utløp enda bestemt.

List of Figures

List of Tables

Nomenclature

η Overall efficiency

η_h Hydraulic efficiency

π 3.14

ψ Pressure Coefficient

θ Blade Wrap Angle

C_m Meridional Velocity[m/s]

Cm_1 Meridional Velocity at inlet[m/s]

D_{shaft} Shaft Diameter[m]

N_p Number of Points on Streamline

N_s Number of Streamlines

$NPSH_a$ Net Positive Suction Head Available[m]

$NPSH_r$ Net Positive Suction Head Required[m]

Q_l Leakage Flow[m^3/s]

Q_{req} Required Volumetric Flow[m^3/s]

C Absolute Velocity in Stationary Frame of Reference[m/s]

Cu Tangential Component of Absolute Velocity [m/s]

g $9.81 m/s^2$

H Pump Head, m

N Rotational Speed, rpm

n_q specific speed

NPSH Net Positive Suction Head[m]

P Power[W]

p Pressure[Pa]

P_{shaft} Shaft Power[W]

Q Volumetric Flow [m^3/s]

R Radius [m]

T Angular Momentum [kgm$^2/s$

U Tangential Velocity of Rotating Frame of Reference[m/s]

W Work[J]

w Relative Velocity with respect to Rotating frame of Reference[m/s]

Contents

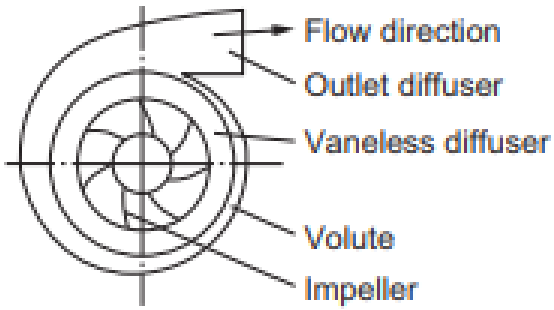

Figure 1: Centrifugal Pump. [15]

4 Introduction

The fast paced development in batteries and electrical engines has led to the possibility to use electric pumps in smaller orbital rockets. Unlike conventional turbo pumps, electric pumps are more flexible, less expensive and much more safe to use. Electrical turbopumps can be designed from a few parameters. The purpose of this thesis to design such a pump based on the pressure rise, volumetric flow and angular velocity of the electric motor.

5 Centrifugal Pumps

[15, pp(1)] classify turbomachines as devices in which energy is transferred either to, or from, a continuously flowing fluid by the dynamic action of one or more moving blade rows. The centrifugal pump is related to the former, namely a device transferring energy to the fluid, where the stagnation enthalpy of the fluid is changed due to the positive work done by the impeller on the fluid. The change in enthalpy is related to pressure change in the fluid. For centrifugal pumps, this corresponds with an increase in the total pressure of the fluid.

The centrifugal pump consists of four main parts, namely impeller, diffuser, volute and outlet diffuser, as seen in Fiugre 1.

5.1 Physical Principles

Turbomachines consist of static and moving parts. The impeller is rotating about the center axis of the pump, while the diffusor and volute are stationary. Hence, when considering the fluid motion a fixed reference frame can be utilized, or alternatively, a reference frame moving with the rotor. The velocity triangle can then be divided into three components. These can be seen in Figure 2 as parallelograms, and in Figure 3 as velocity triangles.

The C component is the absolute velocity of the fluid in the stationary frame of reference. The U component is the velocity of the rotating reference frame, in this case the impeller. Finally, the w component is the relative velocity with respect to the rotating frame. The angles α and β represents the angles between the absolute and the relative velocities respectively. As can be seen from the inlet velocity triangle in Figure 3, $\alpha_1 = 90^o$. The physical

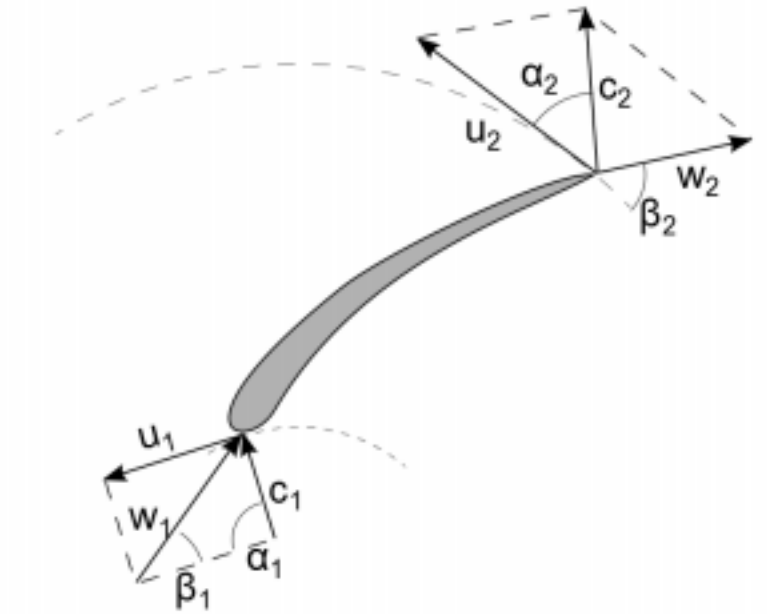

Figure 2: Velocity parallelogram for impeller. [22]

meaning of this is the assumption of zero swirl at the inlet, i.e. $Cu_1 = 0$.

The subscripts 1 and 2 corresponds to the impeller inlet and outlet respectively. By vector calculations, the relationship between the velocities can be described as Eq. **??**:

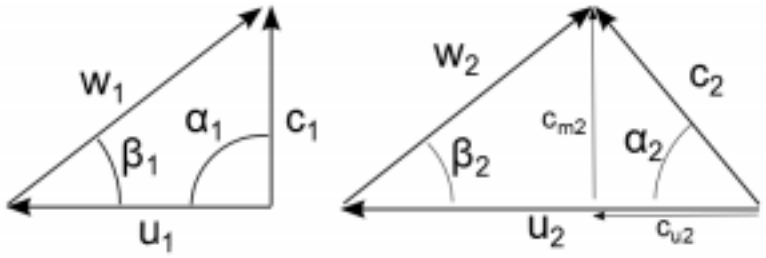

Figure 3: Velocity triangles. [22]

Centrifugal pump theory is based on conservation of momentum [3, pp(30)]. The angular momentum transferred from the impeller to the fluid can be described with the following equation:

$$T = \rho Q(R_2 Cu_2 - R_1 Cu_1) \tag{5.1}$$

which is also known as the "Euler's turbine equation".

The shaft power required to transfer this momentum is given by:

$$P_{shaft} = \rho Q(Cu_2 U_2 - Cu_1 U_1) \tag{5.2}$$

Further on, Eq. 5.3 gives the specific work done by the impeller.

$$W = \frac{P_{shaft}}{\rho Q} = Cu_2 U_2 - Cu_1 U_1 \tag{5.3}$$

The actual useful work done on the fluid by the impeller is lower than the work done by the impeller due to hydraulic losses, which is defined by the hydraulic efficiency coefficient, η_h. An equation solving for η_h i presented in Ch 5.2.1 when calculating the main dimensions. Hence the useful work done on the fluid is calculated using

$$W_h = \eta_h W \tag{5.4}$$

To calculate the energy transferred to the fluid from the inlet of the pump to the outlet, the Bernoulli eqauation:

$$\frac{P_{in}}{\rho} + gz_{in} + \frac{C_{in}^2}{2} + W_h = \frac{P_{out}}{\rho} + gz_{out} + \frac{C_{out}^2}{2} = constant \tag{5.5}$$

is used, where C is the absolute velocity, and z is the geometric height.

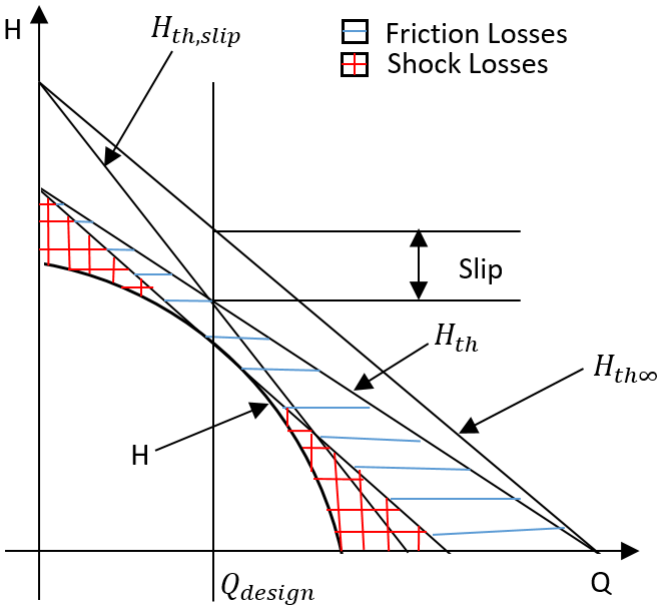

Figure 4: Characteristic Curve

5.2 Pump Characteristics

When designing the impeller of a centrifugal pump, shockless entry is assumed. Shockless entry can only be achieved when the pump is operating with the head and flow it is designed for. Again, considering an impeller with infinite number of infinitely thin blades, the theoretical head from Eq. 5.9 can, through vector operations in Figure 3 be rearranged to

$$H_{th\infty} = \frac{U_2}{g}\left(U_2 - \frac{C_{m2}}{tan(\beta_2)}\right) \tag{5.6}$$

As Cm_2 is directly linked to the volumetric flow, Q, through Eq.5.7

$$C_{m2} = \frac{Q}{A_2} \tag{5.7}$$

Eq. 5.6 clearly states that the maximum head achievable is at zero flow, i.e. $Q = 0$, and $H_{th\infty} = \frac{U_2^2}{g}$.

Figure 4 shows a general characteristic curve of a centrifugal pump. As the figure shows, if Q increases or decreases from design point, shock losses will occur.

5.3 Main Parameters

5.3.1 Head

When dealing with turbo machines, a common way to express energy transfer is by the means of head, H. This variable relates the energy to a column height of the same fluid, and is expressed by Eq. 5.8:

$$H = \frac{W}{g} = \frac{P_{out} - P_{in}}{\rho g} + z_{out} - z_{in} + \frac{C_{out}^2 - C_{in}^2}{2g} \tag{5.8}$$

If no hydraulic or frictional losses were present in the impeller, all the power would be transferred to the fluid by the impeller. The theoretical head, i.e. no losses, is given by Eq.

$$H_{th} = \frac{C_{u2}U_2 - C_{u1}U_1}{g} \tag{5.9}$$

Hence, if the assumption of zero swirl at the inlet holds, Eq.5.9 becomes

$$H_{th} = \frac{C_{u2}U_2}{g} \tag{5.10}$$

For a given hydraulic efficiency, the actual head realizable can be determined by

$$H = \eta_h H_{th} \tag{5.11}$$

Centrifugal pumps for rocket engines have been developed for head requirements ranging from 450 to around 3650 meters fluid column when dealing with fluids of conventional density, and even up to 61 000 meters when dealing with hydrogen pumps [2].

5.3.2 Flow Rate

The flow rate is the desired volumetric flow, Q, which the pump is designed to deliver. Flow rates for rocket engine pumps range from 0.7 l/s to 1900 l/s, with the majority of the pumps operating between 75 to 750 l/s [2].

The actual flow rate through the impeller is larger than the flow rate specified at the beginning of the design procedure, due to leakage through annular seals, Q_l, and leakage between the impeller and the stationary parts, i.e. volute and diffuser. Hence, when designing a centrifugal pump, the designer has to compensate for these secondary flows The required flow rate through the impeller is decided using Eq. from Gulich [1, pp(70)]:

$$Q_{req} = Q + Q_l \tag{5.12}$$

where Q_{req} is the required flow rate to deliver the desired flow rate, Q.

Karassik [6] proposes a way to estimate the leakage losses through Eq. 5.3.2

$$\frac{Q_l}{Q} = 5\left[\frac{\frac{\delta}{r_R}\left(\frac{r_R}{r_2}\right)^2}{n_q^2 \psi}\right] \tag{5.13}$$

where δ/r_R is the clearance ratio, ranging between 0.001 and 0.002, and r_e/r_2 is the ratio between the eye radius and the tip radius. According to Huzel and Huang [7], p(207), the leakage loss, Q_l lies between 1 to 5% of Q for similar pumps. Since the machining quality δ is not known at this moment, the leakage will be set to 5% of Q, as proposed by Huzel and Huang [7], p(207).

5.3.3 Rotational Speed

The rotational speed, N, is the number of times the impeller revolves about the rotational axis per minute.

5.3.4 Specific Speed

Specific speed is a similarity criterion for pumps as Reynolds number is for pipe flow [3, pp(27)]. Due to the wide range of applications for centrifugal pumps, a relationship combining the main parameters, namely the head, H, the rotational speed, N and the volumetric flow, Q is of great importance. Gulich, [1, pp(82)], defines specific speed as follows:

$$n_q = N \frac{\sqrt{Q_{opt}}}{H_{opt}^{0.75}} \tag{5.14}$$

where Q_{opt} and H_{opt} are the volumetric flow and head at best efficiency point respectively. Another way to define the specific speed is done by Stepanoff [3],p(73):

$$n_s = \frac{N\sqrt{Q_{opt}}}{(gH_{opt})^{0.75}} \tag{5.15}$$

Both Eq. 5.14 and Eq. 5.15 describe the same characteristics of the pump, but it is of great importance to choose the one corresponding to eventual charts or equations when deciding the main dimensions of the pump. Different pump classes corresponding to different specific speeds can be seen in Figure 5.

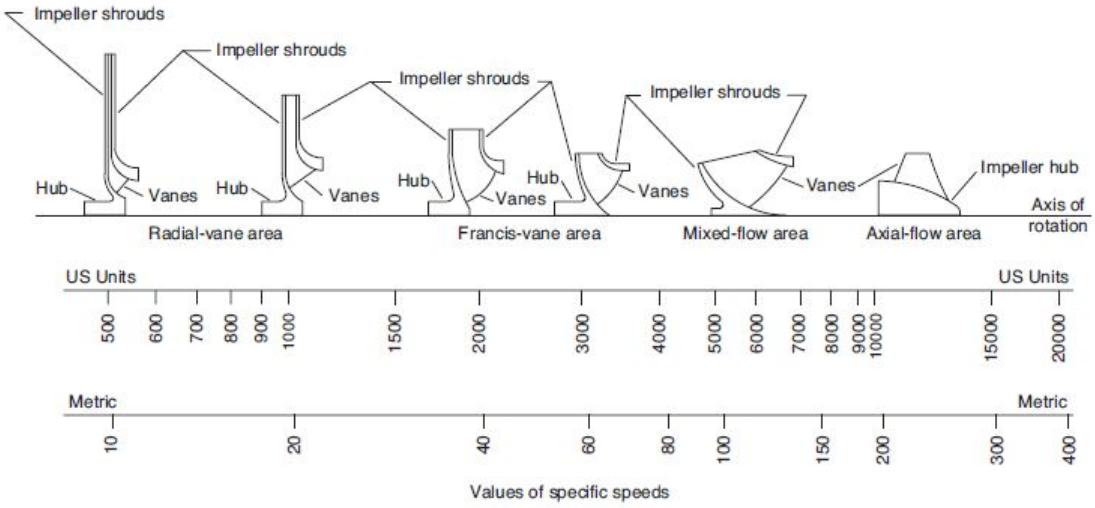

Figure 5: Figure 1: Pump Classification. [4]

As Figure 5 shows, centrifugal pumps lie in the scope of n_q <30, using metric units.

5.3.5 NPSH

When studying centrifugal pumps, a crucial parameter to consider is the net positive suction head (NPSH), which is defined by [3, pp(28)], as the gage reading in meters taken on the suction nozzle referred to the pump center line, minus the gage vapor pressure in meters corresponding to the liquid temperature, plus the velocity head at the same point. In mathematical terms, this is expressed as:

$$NPSH = \frac{P_{in} - P_v}{\rho g} + \frac{C_{in}^2}{2g} \tag{5.16}$$

where P_v is the fluid vapor pressure at the given temperature. The net pressure suction head is essential in order to avoid cavitation [1, pp(45)]. When the fluid is obstructed by the leading edge of the blade, excess velocities causes the local pressure to drop in correspondence with the Bernoulli equation 5.5. If the local pressure drops below the vapor pressure, the fluid will evaporate, causing gas bubbles to form and travel along the flow in the impeller. As the pressure increase throughout the impeller, these bubbles will implode, resulting in shockwaves. If extensive cavitation occurs, this can impair the the performance of the flow, and even shatter the impeller. According to Gulich [1, pp(45)], we distinguish between net pressure suction head required ($NPSH_r$), which is the net pressure suction head required to avoid, or partly avoid cavitation, and the net pressure suction head available ($NPSH_a$), which is the net pressure suction head available at the pump inlet.Equation 5.16 easily reads the importance of designing the impeller inlet diameter such that such that $NPSH < NPSH_a$, since $NPSH$ is a function of the velocity squared.

Another important parameter regarding cavitation prediction is the suction specific speed, N_{ss}. As for the specific speed n_q, geometrically similar pumps also have the same value for N_{ss}. By substituting H in Eq. 5.14 with $NPSH_r$ Eq.5.17 gives the relationship between N_{ss} and $NPSH_r$

$$N_{ss} = N\frac{\sqrt{Q}}{NPSH_r^{0.75}} \tag{5.17}$$

Huzel & Huang [16, pp(170)] recommend inducers for centrifugal pumps with N_{ss} greater than 10 000. Inducers are axial impellers in front of the centrifugal impeller, which serves the purpose of raising the main impeller inlet pressure such that cavitation is at a minimum. Rocket propellant pumps can reach N_{ss} of over 100 000, and are thus dependent of inducers to operate without severe cavitation. However, for the pump in this thesis, an effort has been made in order to operate the pump without an inducer.

5.3.6 Power and Efficiencies

The exact efficiency of the pump is difficult to determine without actually testing the pump. Therefore, efficiencies based on similar pumps are used to estimate losses in the pump. The losses regarding centrifugal pumps are mainly divided into seven different categories, according to Gülich [1], p(84). These are:

- Mechanical losses
- Volumetric losses
- Disk friction losses
- Similar friction losses
- Interstage leakages in multistage pumps
- Hydraulic losses
- Fluid recirculation losses

Thus, when calculating the power required from the electric motor to operate the pump, all the losses mentioned above have to be accounted for. The total efficiency, η, is the product of all the efficiencies in the pump. Gulich [1, pp(142)] proposes two empirical formulas dependent on the specific speed to estimate the total efficiency,η and the hydraulic efficiency ,η_h through Eq.5.19 and Eq. 5.21 respectively:

$$m = 0.1a(\frac{Q_{ref}}{Q})^{0.15}(\frac{45}{nq})^{0.06} \tag{5.18}$$

$$\eta = 1 - 0.095(\frac{Q_{ref}}{Q})^{m} - 0.3(0.35 - log_{10}(\frac{nq}{23}))^2(\frac{Q_{ref}}{Q})^{0.05} \tag{5.19}$$

$$m_h = 0.08a(\frac{Q_{ref}}{Q})^{0.15}(\frac{45}{nq})^{0.06} \tag{5.20}$$

$$\eta_h = 1 - 0.055(\frac{Q_{ref}}{Q})_h^m - 0.2(0.26 - log_{10}(\frac{nq}{25}))^2(\frac{Q_{ref}}{Q})^{0.1} \tag{5.21}$$

where $Q_{ref} = 1$ and $a = 1$ for this particular pump.
Table 1 shows the calculated main parameters for the pump designed in this thesis

Parameter	Value
H	476.6 m
Q	20 l/s
N	12000 rpm
n_q	16.6
η_h	0.84
η	0.71
Motor power	150 kW

Table 1: Main Parameters.

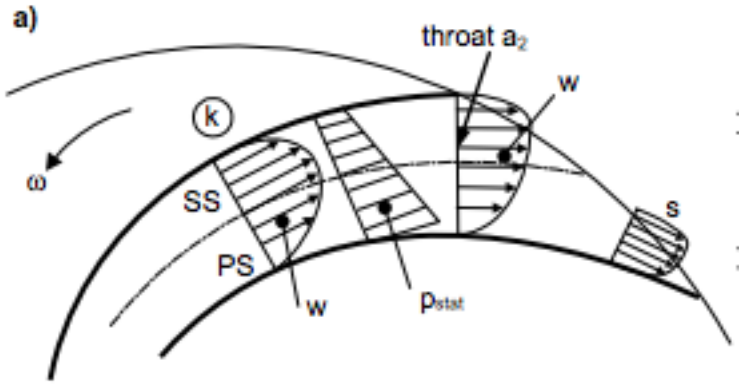

Figure 6: Velocity profile in impeller. [1]

5.3.7 Slip

When applying the theorem of conservation of momentum for head calculations, the average velocities at the impeller inlet and outlet are utilized. However, this does not account for the complex flows occurring inside the impeller channel. As described by Gulich [1, pp(75)], p(75), the forces acting upon the fluid from the impeller blades can be represented as an integral of the pressure and shear stress distributions over the blade surface. As with an airfoil generating lift, this integral cannot be zero in order for the blade to generate a net force on the fluid, thus a pressure difference must be present between the blade suction side and pressure side. As the pressure distribution is coupled with the velocity distribution, this would also result in different velocity distributions between the suction and pressure side, and the flow will therefore not follow the blades exactly. An example velocity profile can be seen in Figure 6, where higher velocities are shown at the suction side, marked SS, opposed to the lower velocities at the pressure side, PS. At the outlet of the impeller, where high pressure flow and low pressure flow converges, the pressure difference vanish through different streamline curvature as seen in Figure 7. The flow angle will deviate from the outlet angle β_2 in favour of the high pressure flow, i.e. resulting in a narrower angle β_2', which can be seen in the new velocity triangle in Figure 8. This phenomenon is called slip, and reduces the hydraulic efficiency of the pump as the Cu_2 component decrease.

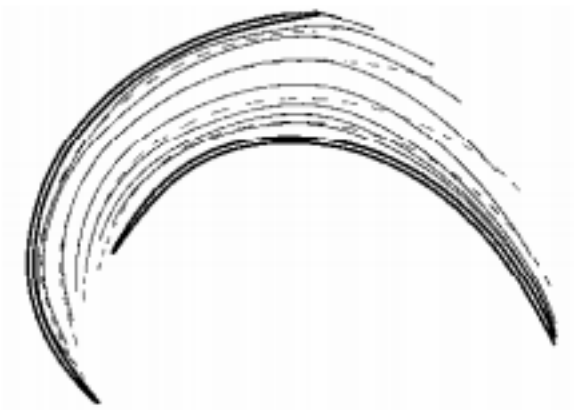

Figure 7: Streamlines in impeller. [1]

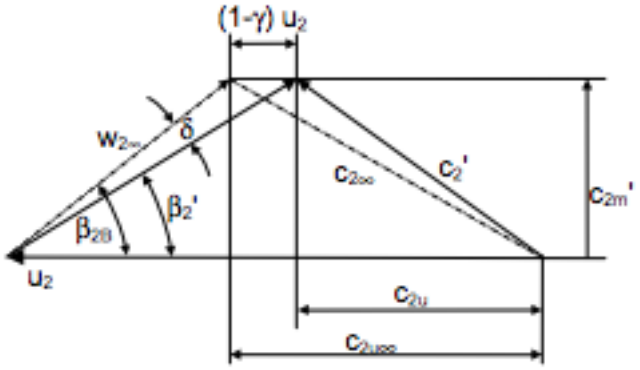

Figure 8: Velocity triangle with slip. [1]

The ∞ subscript in Figure 8 subscript represents a theoretical impeller with infinite number of blades of infinitely small thickness, and therefore no slip. Furthermore, the $'$ superscript represents an impeller with a finite number of blades with thickness greater than zero, i.e. generating slip. The difference between slip and no slip can be expressed through γ which is known as the slip factor. Hence, from Figure 8, and Gulich [1], p(77), the difference between $Cu_{2\infty}$ and Cu_2 can be calculated through Eq. 5.22:

$$Cu_{2\infty} - Cu_2 = (1 - \gamma)U_2 \tag{5.22}$$

As Eq. 5.22 clearly states, a smaller γ results in a greater deviation in the velocities. Oppositely, a slip factor of 1 results in zero slip, or blade-congruent flow.

Although an exact value of the slip factor is difficult to obtain in the design phase, it has to be accounted for when designing a centrifugal pump in order to predict the actual outlet velocities. Several equations and theories have been developed to estimate the slip factor, but it is not in the interest of this thesis to compare different slip theories. Therefore, the slip factor suggested by Wiesner [12] is the only one considered. Eq. 5.23 shows the calculation of the slip factor:

$$\gamma = 1 - \frac{\sqrt{sin\beta_2}}{Z_{La}^{0.7}} \tag{5.23}$$

5.4 Main Dimensions

Once the dimensionless parameters have been calculated, the main dimensions of the pump can be decided based on empirical data. There are numerous ways to calculate these, either through charts or equations dependent on the dimensionless parameters. The dimensions calculated for this thesis are based on the the empirical data found in Centrifugal and Axial Flow Pumps by Stepanoff, [3], with some modifications. Through a set of dimensionless constants, the size of the impeller inlet and outlet can be determined. The three constants K_u, K_{m2} and K_{m1} defined as:

$$K_u = \frac{u_2}{\sqrt{2gH}} \tag{5.24}$$

$$K_{m2} = \frac{Cm_2}{\sqrt{2gH}} \tag{5.25}$$

$$K_{m1} = \frac{Cm_1}{\sqrt{2gH}} \tag{5.26}$$

K_u is known as the speed constant, and it represents the relationship between the peripheral velocity and the pump total head. The constant is chosen based on empirical data presented by Stepanoff [3, pp = 79], as a function of the specific speed. As Stepanoff mentions, a greater speed constant K_u could be chosen when dealing with small pumps in order to overcome the hydraulic losses. When K_u is chosen, the outer diameter D_2 is calculated from the rotational speed

$$u_2 = \omega R_2 \tag{5.27}$$

K_{m2} is the capacity constant is used to calculate the meridional velocity C_{m2} at the impeller discharge. This constant can as well be decided by means of empirical data. Through Eq. 5.28:

$$C_{m2} = \frac{Q}{A_2} = \frac{Q}{(\pi D_2 - z s_u) B_2} \tag{5.28}$$

the outlet height, B_2 can be calculated. s_u is the tangential thickness of the impeller vane at the outlet, and acts as a blockage at the outlet. Hence, thicker vanes decreases the effective outlet area and increase the meridional outlet velocity.

The last constant, K_{m1} defines the entrance velocity. Hence, if the shaft diameter is known, D_1 can be calculated by Eq. 5.29:

$$D_1 = 2\sqrt{\frac{Q}{\pi C m_1} + (\frac{D_{shaft}}{2})^2} \tag{5.29}$$

When the main dimensions of the pump are determined, the inlet and outlet angles β_1 and β_2 can be calculated. Referring to Figure 3, β_1 and β_2 are defined through Eq. 5.30 and 5.31, respectively.

$$\beta_1 = \arctan\left(\frac{C_{m1}}{U_1}\right) \tag{5.30}$$

$$\beta_2 = \arctan\left(\frac{C_{m2}}{U_2 - C_{u2}}\right) \tag{5.31}$$

As mentioned in Section 5.1, β_1 is calculated under the assumption of zero swirl at the inlet. The main dimensions and angles for the pump can be seen in Table 1:

Parameter	Value
D_1	2.39 cm
D_2	16.18 cm
B_2	0.32 cm
β_1	24.2^o
β_2	28^o

Table 2: Main Dimensions and Angles.

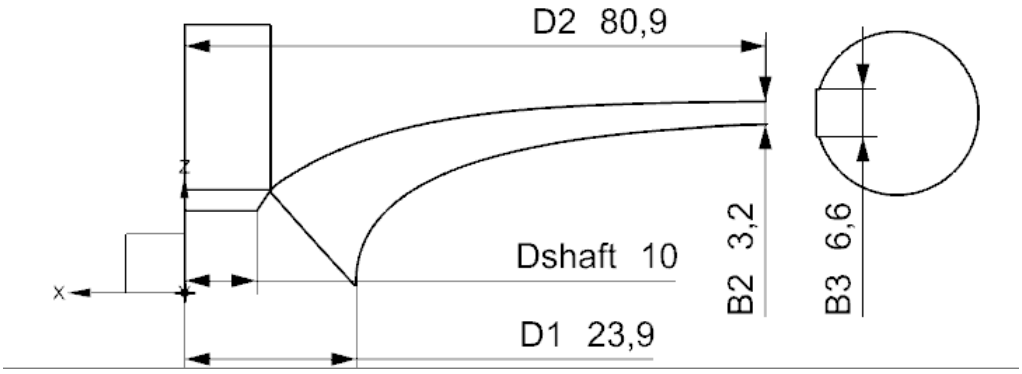

Figure 9: Pump Dimensions

Figure 9 shows the main dimensions of the pump with the volute inlet width B_3, which will be discussed later:

6 Design Process

The design process has been an iterative process in order to satisfy the given head, while not exceeding the power available from the motor. Zero cavitation was also set as a criteria for successful design. The main steps in the iterative process can be seen in Figure 10

The impeller design is done through a Matlab code generated in this thesis. After the coordinates for the blade, hub and shroud have been calculated, the The design code is based on the method described in [5], with some modifications in order to fit the design for this pump. The method is described step by step in the following subsections:

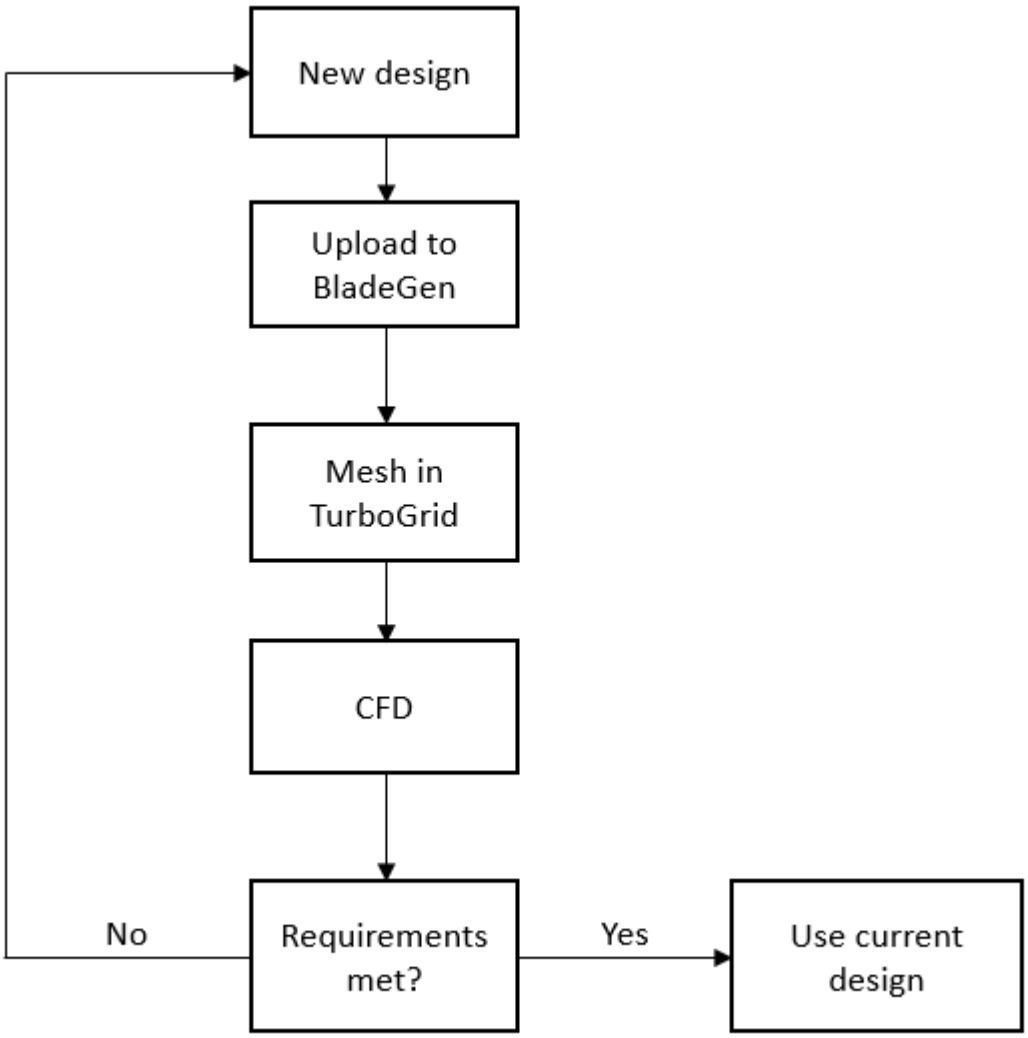

Figure 10: Iterative Process

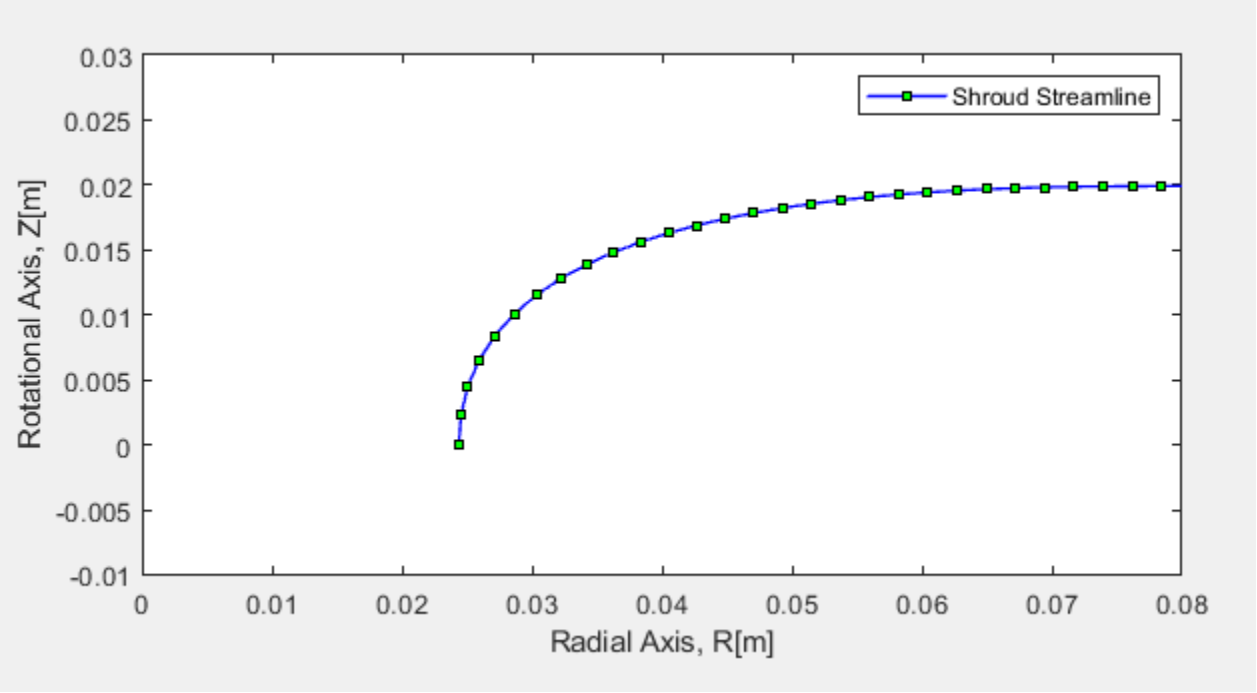

Figure 11: First Streamline.

6.1 Impeller Design

6.1.1 Design of Meridional Path

The meridional path of the pump decides the hub and shroud curvature. The first streamline is designed using a Bezier curve with R_1, R_2 and Z_e as parameters, where Z_e is the depth of the impeller, given by equation (6.1) from Gulich [1]:

$$Z_e = (D_2 - D_1)(\frac{n_q}{47})^{1.07} \tag{6.1}$$

The resulting streamline can be seen in Figure 11, and represents the shroud contour of the impeller. This streamline is the base for calculating the remaining streamlines.

When the first streamline is defined, the endpoints of the remaining streamlines can be calculated by assuming the flow rate to be equal per between each streamline [5, pp(16)].

By using the principle of mass conservation, Eq.6.2:

$$C_{m1}A_1 = C_{m2}A_2 \tag{6.2}$$

where

$$A_1 = \pi R_1^2 \tag{6.3}$$

and

$$A_2 = 2\pi R_2 B_2 \tag{6.4}$$

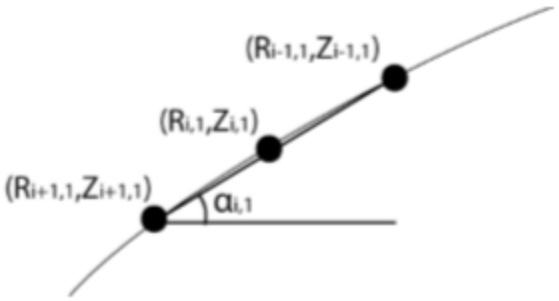

Figure 12: Defining α. [5]

the height of the outlet, B_2 can be calculated, since Cm_1 and Cm_2 are set by the designer.

The endpoints of the streamlines are now known, by R_1, R_2, Z_e and B_2. By choosing the number of streamlines, N_S, the distance between Z_e and $Z_e + B_2$ is discretized by N_s streamlines, which represents the streamlines at the outlet of the impeller. Calculating each streamline is done by the following process from [5], p(16-18):

- Discretize the first streamline into N_p, and define the angle α, as shown in Figure 12: where α is defined as:

$$\alpha_{i,1} = tan^{-1}\left(\frac{Z_{i-1,1} - Z_{i+1,1}}{R_{i-1,1} - R_{i+1,1}}\right) \tag{6.5}$$

- Define the following variables:

$$r_{i,1} = \frac{R_{i,1} + R_{i,2}}{2} \tag{6.6}$$

$$A_{i,1} = 2\pi r_{i,1} b_{i,1} \tag{6.7}$$

$$b_{i,1} = \frac{R_{i,2} - R_{i,1}}{sin(\alpha_{i,1})} \tag{6.8}$$

  and rearranging Eq. 6.6, 6.7 and 6.8 to obtain Eq.

$$R_{i,2} = \sqrt{R_{i,1}^2 + \frac{A_{i,1} sin(\alpha_{i,1})}{\pi}} \tag{6.9}$$

  Finally, the last equation:

$$Z_{i,2} = Z_{i,1} - b_{i,1} cos(\alpha_{i,1}) \tag{6.10}$$

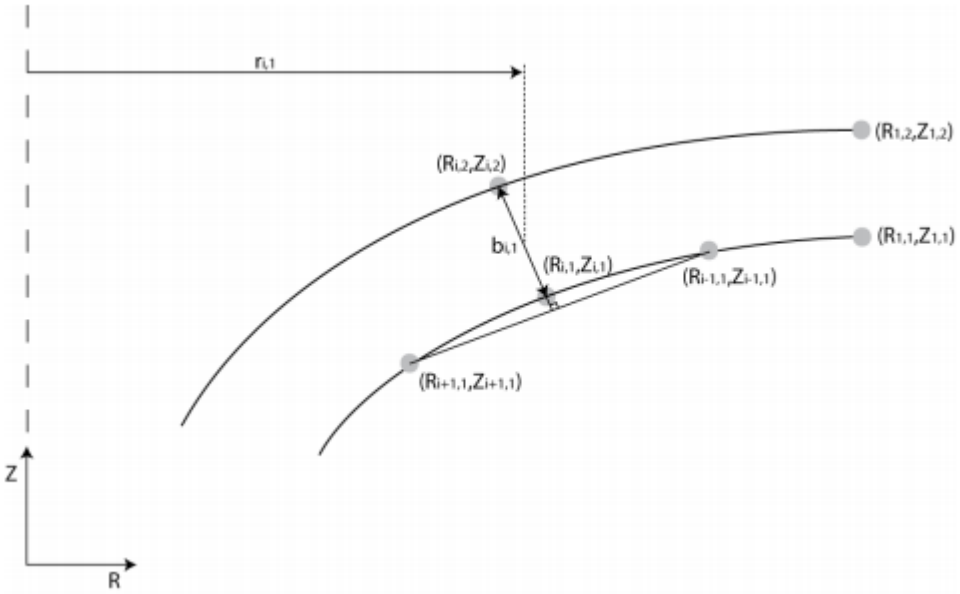

Figure 13: Solving Second Streamline. [5]

The area $A_{i,j}$ between the streamlines can be calculated by assuming the change in meridional velocity occurs linearly. The remaining streamlines are calculated in the same manner as the second streamline.

Figure 14 shows the final meridional path of the impeller blade. Here, the streamlines have been cut according to [1]

After calculating the meridional path of the impeller, the radial view has to be calculated. The procedure starts by defining a new plane with the variables G and H as variables. G is defined by the length of a streamline in the meridional path, while H is defined as the length of a streamline in the radial plane, and must not be confused with the head, H. As the coordinates in the meridional plane are known from the previous section, G, can be calculated using Pythagoras, as Eq 6.11 shows:

$$G_{i,j} = G_{i-1,j} + \sqrt{(R_{i-1,j} - R_{i,j})^2 + (Z_{i-1,j} - Z_{i,j})^2} \tag{6.11}$$

To calculate length of the streamline in the radial plane, the distribution of the blade angle β has to be known. β is given at each point through the impeller from Eq 6.13

$$\beta = arctan\left(\frac{C_m}{U - C_u}\right) \tag{6.12}$$

C_m is as mentioned assumed to change linearly throughout the impeller, and the tangential velocity U is calculated by $U = \omega r$, where ω is the angular velocity, and r is the radius at the given position. C_u and the β distribution are unknown.

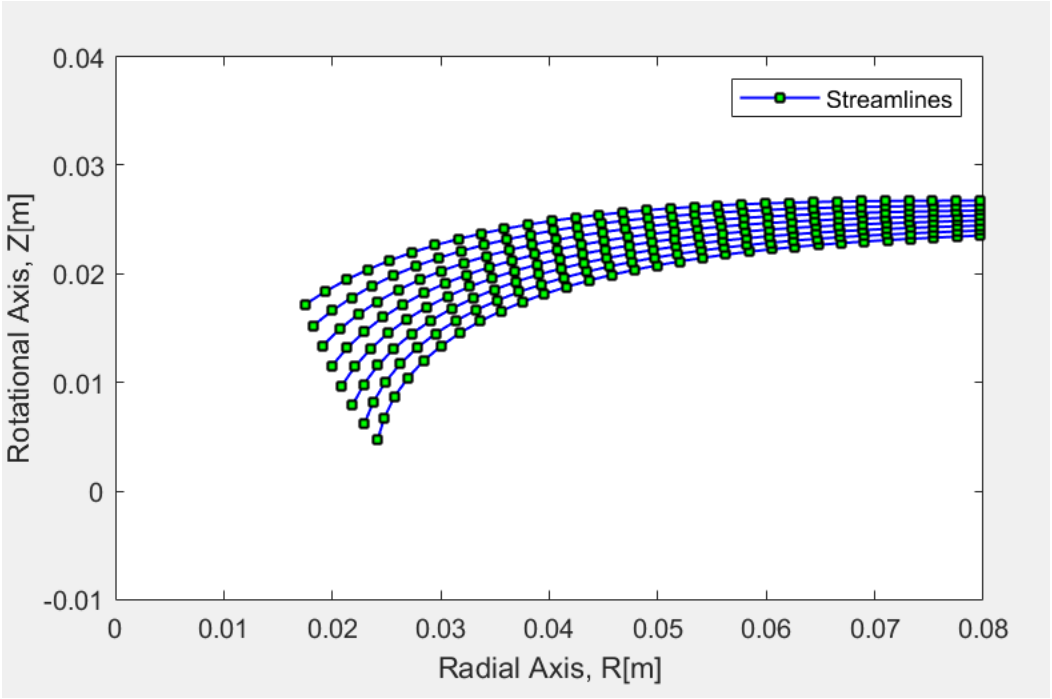

Figure 14: All Streamlines

6.1.2 Design of Radial Plane

The β distribution has been calculated as done by [8]. [8] defines the angle distributions along any meridional streamline as a quadratic function:

$$\beta_e = al^2 + bl + c \tag{6.13}$$

, where a,b and c are coefficients, and l is the length to on the meridional streamline to point e, where β_e is calculated. At $l = 0$, $\beta_e = \beta_1$ and at $l = l_0$, $\beta_e = \beta_2$, i.e. the inlet and outlet respectively. Hence, the coefficients b and c can be eliminated. Equation 6.13 can then be written as:

$$\beta_e = \beta_1 + \frac{l(\beta_2 - \beta_1)}{l_0} + al(l - l_0) \tag{6.14}$$

The distribution coefficient a can be found by an iterative process:

- Guess a value for a
- Solve Eq. 6.16
- If the wrap angle, θ which is defined as the third polar coordinate, is satisfied, stop iteration. If not, choose another value of a

Since β is known at each point along the streamline through Eq. 6.14, the radial length H can be solved using Eq. 6.15

$$\Delta H = \frac{\Delta G}{tan\beta} \tag{6.15}$$

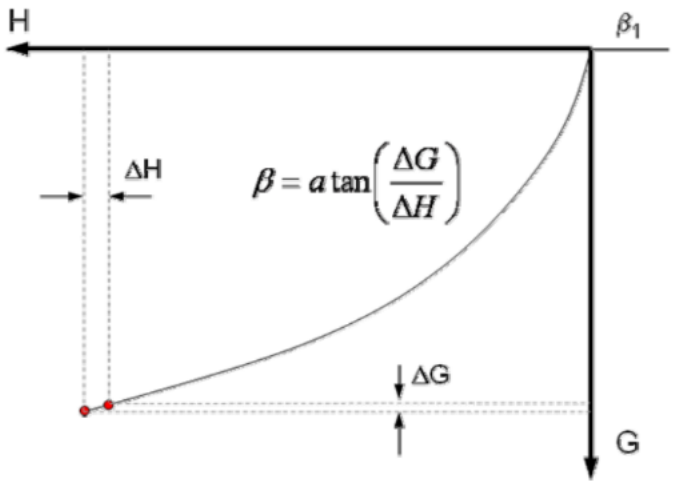

Figure 15: Relationship Between H,G and β. [5]

The relationship between G, H and β can be seen in Figure 15:

The final step in creating a 3D blade from a 2D meridional flow path is calculating the blade wrap angle, θ. The blade wrap angle is given by Eq. 6.16

$$\theta = \int_0^{G_{end}} \frac{dG}{tan\beta} \tag{6.16}$$

where G_{end} is the end point of the streamline. By differentiation and discretization of Eq. 6.16, and combining with Eq. 6.15, Eq.6.17 arises:

$$\Delta\theta = \frac{\Delta H}{R} \tag{6.17}$$

Figure 16 shows the correlation between θ, H and R:

Studies done by [8], a large blade wrap angle has positive effects on both efficiency and head due to the smooth increase in the pressure gradient, but if the wrap angle is too large, friction losses will become substantial. However, if the wrap angle is too small, the impeller cannot operate stably [17].

The radial view of the impeller can be seen in Figure 17. As the figure shows, the wrap angle is 165^o. This is considerably larger than what Gulich [1, p(354)] suggests for six vanes. The reason for the large wrap angle is the small ratio D_1/D_2, which results in relatively long vanes, hence the large wrap angle.

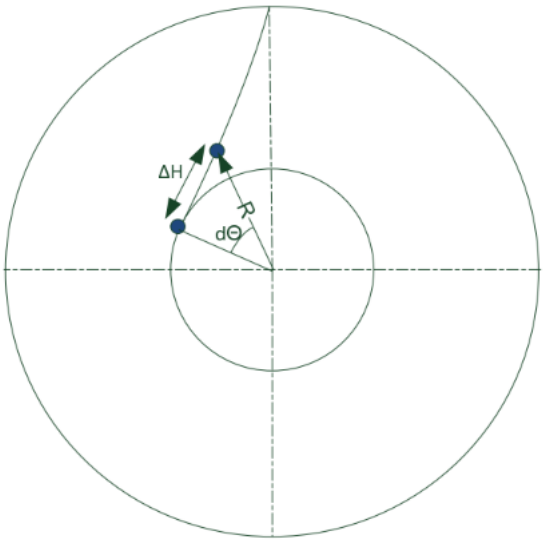

Figure 16: Correlation between θ, H and R. [5]

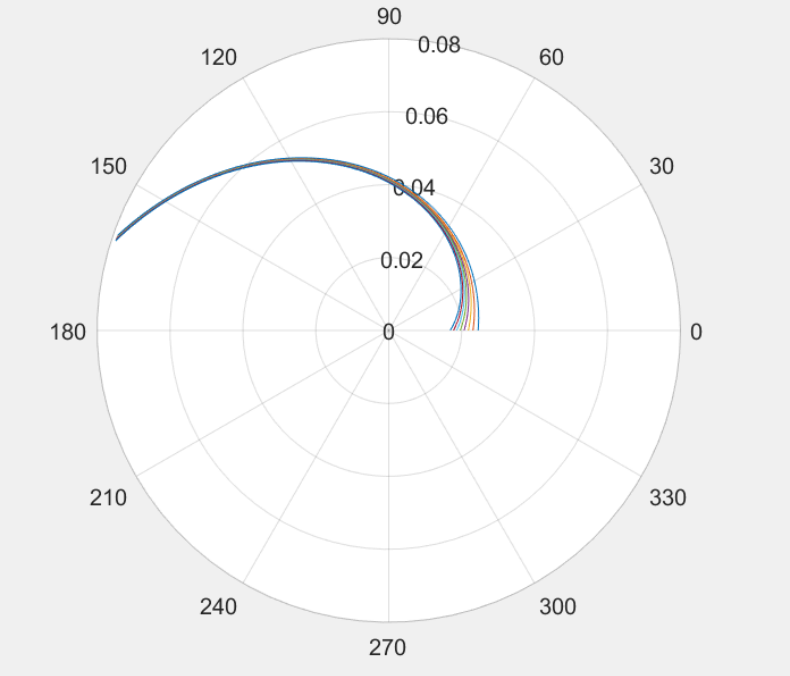

Figure 17: Radial View

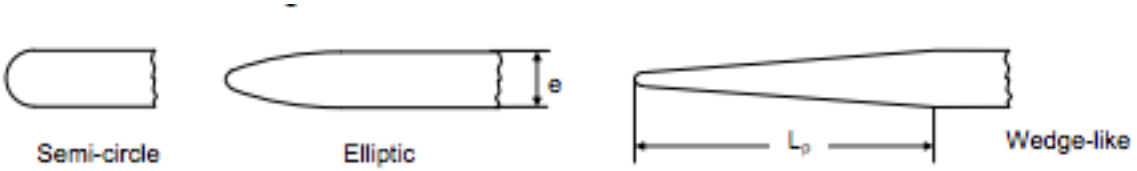

Figure 18: Leading Edge Profiles. [1]

6.1.3 Blade Thickness

The blade needs to withstand the forces acting upon it throughout the impeller, and it is the blade that transfer the power from the shaft to the fluid. Therefore it is of utmost importance that the blade is thick enough, so it does not break under the operating conditions. The hydraulic forces acting on the blade are both static and dynamic. The static forces is due to the pressure difference between the pressure side and the suction side, while the dynamic forces comes from pressure pulsations inside the impeller.

Gulich [1, p(347)] suggests a blade to outlet diameter ratio, $t/D2$ between 0.016 to 0.022, where the upper range is applied for pump heads above 600 meters. The head for this particular pump

6.1.4 Incidence

The incidence angle i is the angle at which the flow deviates from encountering the leading edge perpendicularly. If $i > 0$, shock losses will occur at the leading edge, and additional fluid is displaced due to the increase in blade blockage

6.1.5 Leading Edge

The shape of the leading edge is of crucial, since the leading edge has great influence on cavitation, pressure distribution and separation [13]. Gulich [1, p(347)], proposes three different leading edge profiles, as seen in Figure 18:

The semi-circle profile generates high local velocities and correspondingly very low pressure regions at the leading edge. This implies poor characteristics regarding cavitation, and semi-circle profile is according to Gulich [1, p(347)], only acceptable in pumps with low requirements.

In contrast to the semi-circle, the wedge-like profile does not generate such high peaks of excess velocities as the semi-circle due to the long gradual increase in area which the flow has to flow around. However, if the incidence angle is not zero, also this profile will generate high excess velocities. In addition, this profile has unfavorable characteristics with regard to strength, and thereby increases the risk of blade cracking [1, p(347)].

The elliptic has shown to provide favourable pressure distributions, and has lower sensitivity to incidence [1, p(347)], and will be utilized for this pump.

6.1.6 Trailing Edge

The trailing edge has to be designed in such a way that it generates a low amplitude vortex shedding and a frequency that does not correspond to any natural frequencies [21].

6.2 Diffuser

The diffuser is a vaneless or vaned section between the impeller and the volute, and its purpose is to increase the efficiency by ensuring a more gradual expansion than if the flow was ejected directly into the volute. According to [**?**], the flow in vaneless diffusers undergo large friction losses, and it is therefore preferable with vaned diffusers in rocket propellant pumps.

The hydraulic losses from the diffuser can be calculated by Bernoulli's equation with losses [1, pp(27)]:

$$c_p = \frac{p4 - p3}{\frac{\rho}{2}c_3^2} = 1 - \frac{1}{A_R^2} - \zeta_{3-4} \tag{6.18}$$

C_p is the pressure recovery coefficient and $A_R = \frac{A_4}{A_3}$ is the area ratio between the diffuser inlet and outlet. ζ_{3-4} is the loss coefficient which accounts for the losses in the diffuser. By comparing the diffuser with an ideal diffuser where no losses occur, C_{pid}, an expression for the diffuser efficiency can be defined as Eq. 6.19 [1, pp(30)]:

$$\eta_D = \frac{C_p}{C_{pid}} = \frac{C_p}{1 - \frac{1}{A_R^2}} \tag{6.19}$$

For a given A_R, C_p can be found by empirical data given by [1, p(28)].

The pump designed in this thesis is a volute pump, hence the diffuser is the vaneless area between the pump and the volute.

6.3 Volute

The volute, or spiral casing, is a curved funnel collecting the fluid after it is discharged from the diffuser. While the impeller transfer energy to the fluid, the volute can only reduce the energy due to friction and mixing losses. It is therefore important to design the volute so that such losses are minimized.

When dealing with centrifugal pumps with low specific speeds, such as the one in this thesis, the losses in diffuser and volute are dominating compared to the losses in the impeller according to Gulich, [1], p(163).

The most common way to calculate the area of the volute is by conservation of angular momentum

where the assumption of Eq. 6.20:

$$Cur = Cu_2r_2 = constant \tag{6.20}$$

gives the basis of Eq. 6.21:

$$\int_{r_z}^{r_A} \frac{b}{r} dr = \frac{Q_{req}\epsilon}{360^o Cu_2 r_2} \tag{6.21}$$

where ϵ denotes the circumferential position. Each cross-section of the volute has to satisfy Eq. 6.21 for the conservation of angular momentum to be fulfilled.

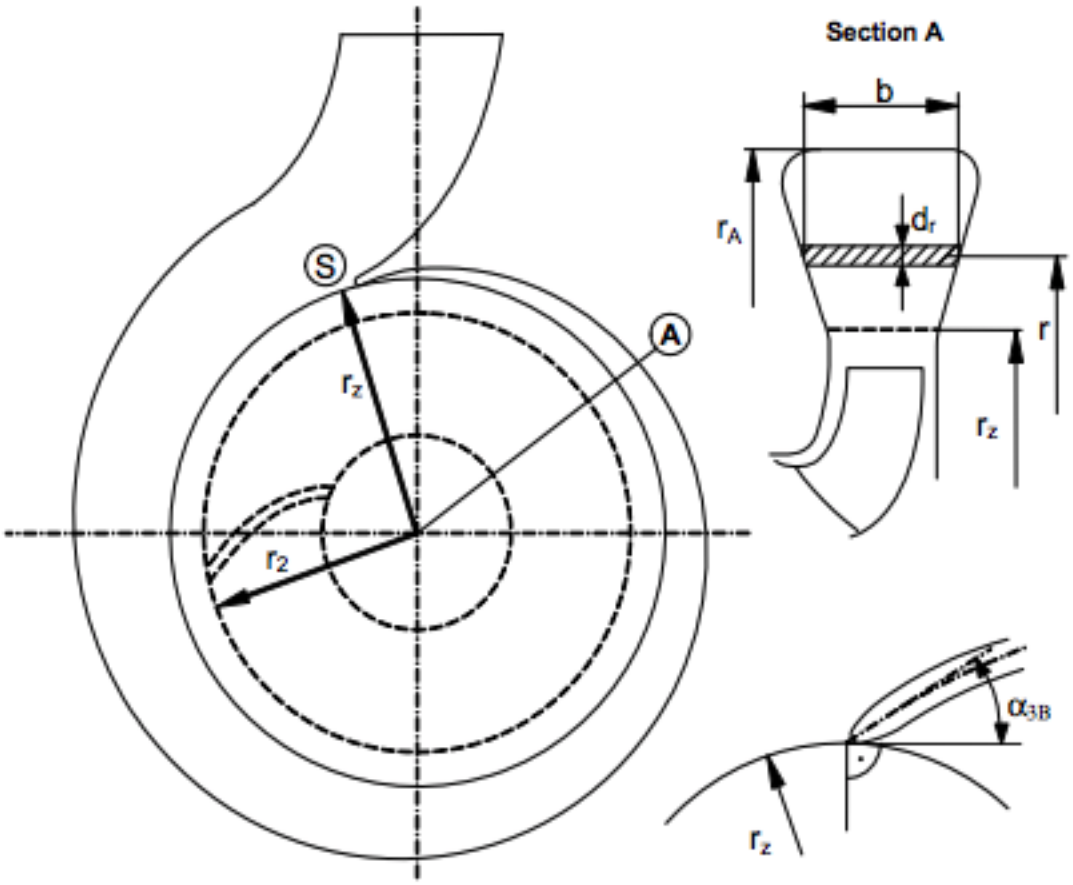

Figure 19: Volute Explanation. [1]

Figure 19 shows the axial view of the volute, to the left and the radial view to the top right. According to Gülich [1], p(103), the losses in the volute become minimal if designed according to Eq. 6.21.

The end section of the volute is often equipped with a diffusing element, i.e. the volute area continues to increase after point S in Figure 19. The reason for this is to decrease the velocity, and thereby decreasing the friction losses further. The volute consists of several elements which determine the hydraulic characteristics. Stepanoff [3], p(111) defines these as the volute areas $A(\epsilon)$, the volute angle α_v, volute width b_3 and the volute base circle D_3.

6.3.1 Volute areas

The end cross-section of the volute, marked by S in Figure 19 is the only area of the volute where the total pump capacity passes through. At any other section of the volute, only fractions of the total flow Q pervade. This implies a gradual increase in the cross-section area throughout the volute.

The volute starts and ends at the same position. This is called the volute tongue, or cut-water [1], p(111). Due to the non-zero distance between the impeller and the volute, some of the flow will recirculate between the tongue and the impeller. Recirculation will also happen between the impeller shrouds and the casing due to the gap.

When calculating the velocity in the volute, and thereby the volute area, the analysis will be done considering the best efficiency point only. Due to leakage, the capacity through the volute will be smaller than what the impeller discharges by the amount of leakage between the impeller and the volute.

An alternative method to using conservation of angular momentum is by use of constant velocity. The average velocity in the volute is calculated by Stepnaoff [3], p(112) as:

$$C_3 = K_3\sqrt{2gH} \tag{6.22}$$

where K_3 is an experimental design factor determined by the specific speed of the pump. This factor can be decided from [3, p(113)].

Although the average velocity can be determined through Eq. 6.22, the velocity distribution across any cross section is non-uniform. According to Stepanoff [3], p(112), the maximum velocity at any cross section in the volute is at the impeller periphery, and the velocities tends to decrease when approaching the volute walls.

Due to the absolute velocity being radially outwards, the flow in the volute is complicated. Depending on whether the volute is symmetrical or asymmetrical, double or single vortices can occur respectively.

The shape of the volute cross-section is also a factor that can either improve or impair the hydraulic efficiency. Due to the simplicity in design, a circular shape has been chosen for this pump.

Figure 9 shows the main dimensions of the final pump design. Z is the rotational axis. B_3 has been chose as $2B_2$ in compliance with [3]. The same goes for D_3, which has been set to $(1 + 0.085)D2$.

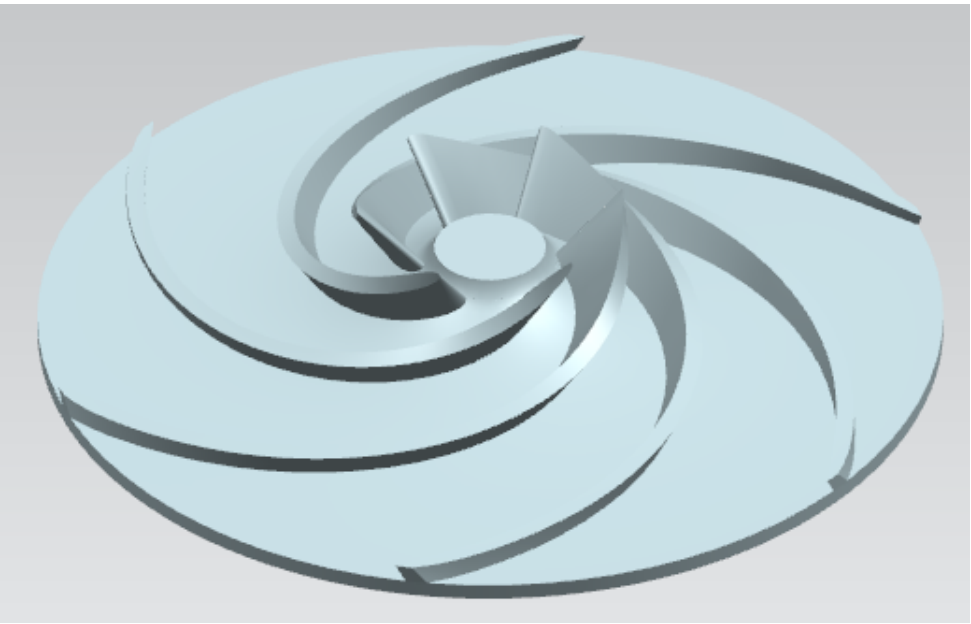

Figure 20: Impeller Without Shroud

7 Final Design

8 CFD Theory

Computational fluid dynamics (CFD) is an outstanding tool used predict the behaviour of the fluid. It is very useful in the field of turbomachinery in the way that hydraulic efficiency, head generation, cavitation and fluid motion can be predicted before the physical model is built and tested. Although the actual fluid behaviour can only be determined through physical testing of the model, numerous experiments has shown good correlation between the numerical models and physical testing.

8.1 Mesh Generation

The impeller model has been uploaded to Ansys TurboGrid. Turbogrid is created especially for generating meshes for turbomachinery, and uses a structured grid to create a high quality mesh. TurboGrid has been used in numerous numerical experiments, with great success, and the opportunity of mesh scaling makes it easy to perform a mesh sensitivity study.

When performing a CFD, it is of great importance to ensure that the solution is independent of the mesh. Hence, starting with a coarse mesh, and refining until the solution has converged is something that should be done for every simulation using CFD

8.1.1 Inflation Layers

In order to obtain a high enough resolution at the wall boundaries, while still avoiding to refine the entire mesh, inflation layers are often used while conducting CFD.

When dealing with viscous fluid flow, the no-slip condition at the walls will lead to lower velocity in the vicinity of the wall, thus generating larger gradients parallel to the wall in these regions. To ensure that these changes are calculated correctly throughout the computations, refinement of the mesh is often required here.

8.2 Turbulence Modelling

If a turbulent flow was to be simulated down to the last detail, a tremendous amount of computer power would be required. Therefore, a vast variety of turbulence models has been developed to model parts of the flow. It is especially the boundary layers, which starts with a viscous inner layer, a mixed layer and a turbulent layer that has to be modelled. For this work the K-ϵ model has been utilized.

8.2.1 K-ϵ Model

K-ϵ model is based on the transport equations for the turbulent kinetic energy,k, and the dissipation rate, ϵ. K is derived from the exact solution of the transport equation for K, while ϵ is

When specifying the grid resolution at those boundaries, it is common to speak in terms of y^+, which is defined by Eq. 8.1:

$$y^+ = \frac{\rho y u_\tau}{\mu} \tag{8.1}$$

where y is the distance from the wall to the first node, and u_τ is the friction velocity, given as a relationship between the wall shear stress τ_w and the density ρ, by Eq. 8.2:

$$u_\tau = \sqrt{\frac{\tau_w}{\rho}} \tag{8.2}$$

According to the mesh has to be refined such that $30 < y^+ < 300$ for the $k - \epsilon$ model. However, [9] states that when using the CFX-solver, there is no lower limit for y^+. If the y^+ value is smaller than the lowest value previously mentioned, CFX uses scalabale wall functions to set the y^+ value correctly. Hence, when refining the mesh, the only consideration is to keep the value small enough, although very small values would imply a waste of mesh elements.

9 Numerical Model

The simulations accomplished throughout this thesis are divided into two main tasks:

- Impeller
- Full simulation of inlet, impeller, diffuser and volute

The following subsections will present the setup for each simulation.

9.1 Impeller

The impeller simulation is the most important one, due to the fact that it is through the impeller the energy transfer occurs. If the impeller does not give the required results, there is no point in simulating the entire pump, since the diffuser and volute can only decrease the efficiency of the pump.

9.1.1 Impeller Mesh

The impeller was meshed using TurboGrid as mentioned in section 8.1. Five simulations with increasing mesh refinement has been performed.

Figure 21 shows the mesh of one blade passage of the impeller.

Inflation layers, as explained in section 8.1.1, has been generated at the wall boundaries. The wall boundaries, as s

9.1.2 Boundary Conditions

The boundary conditions chosen for simulation of the impeller can be seen in Table 5:

Due to symmetry, only one blade and passage has to be simulated, at least for the purpose of this thesis, hence saving computational time required to simulate the impeller. The rotational periodicity boundary conditions indicates the beginning and end of the periodic domain. These boundaries can be seen as rotating arrows in Figure 23:

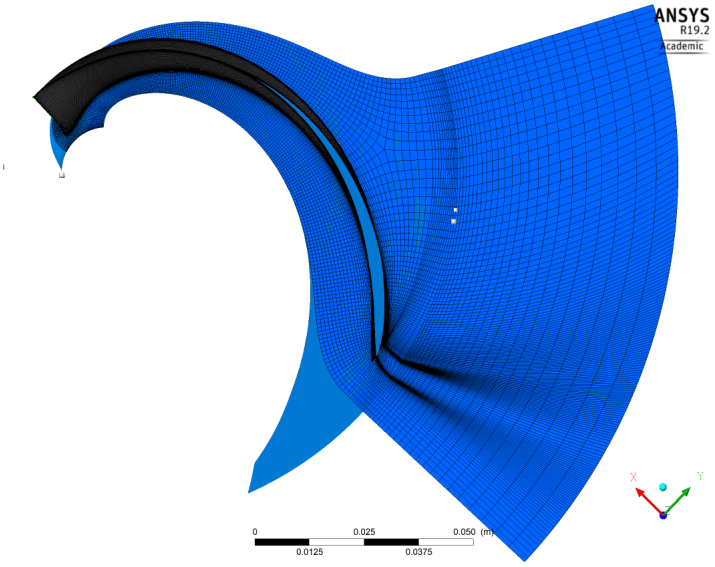

Figure 21: Impeller Mesh

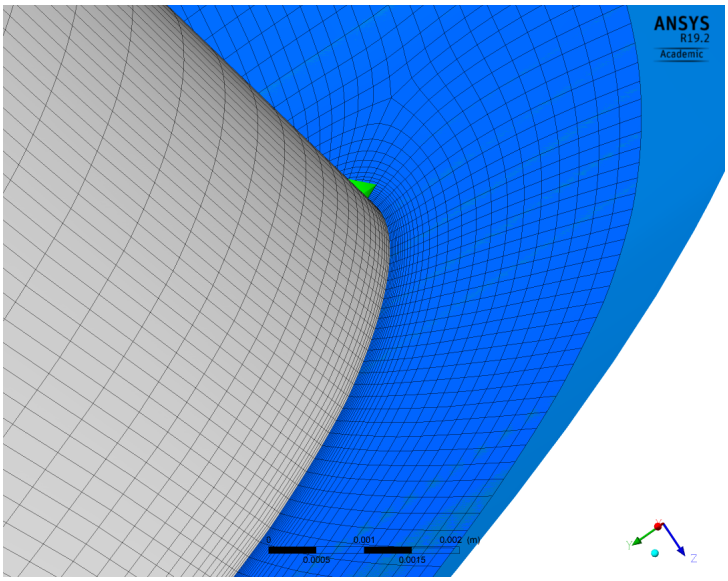

Figure 22: Inflation Layers

Boundary	Boundary Condition
Inlet	Total Pressure: 4.5 [bar]
Blade	No-Slip Wall
Periodic	Rotational Periodicity
Hub	No-Slip Wall
Shroud	No-Slip Wall
Outlet	Mass Flow: 17.1 [kg/s]

Table 3: Boundary Conditions.

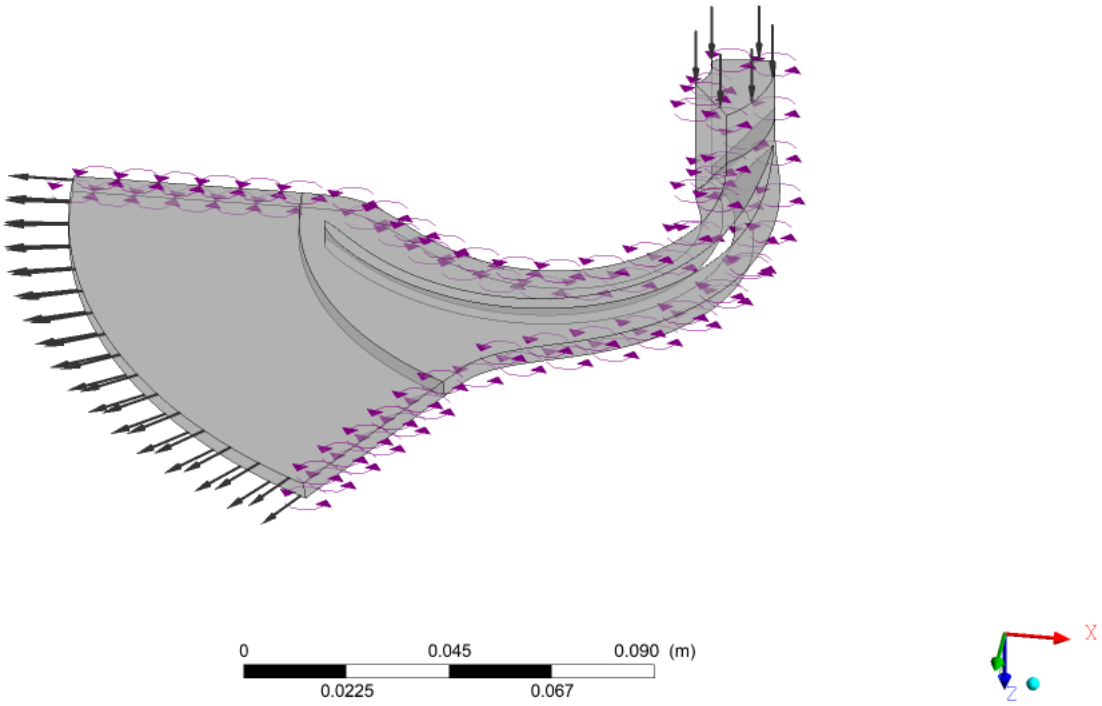

Figure 23: Boundary Conditions

Property	Value
Density	855.6 kg/m^3
Kinetic viscosity	$2.5 * 10^{-6} m^2/s$
Specific Heat Capacity	2842 J/kg*k
Dynamic Viscosity	$2.14 * 10^{-3}$ Pa s

Table 4: Fluid Properties.

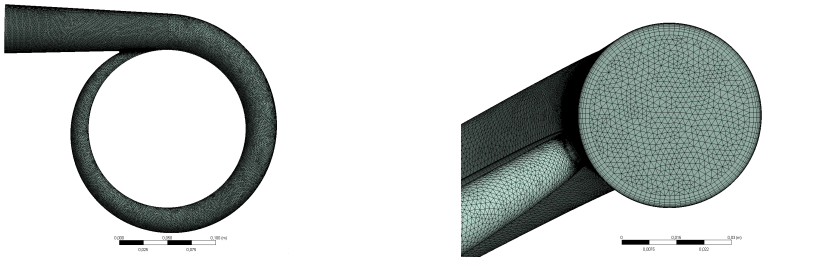

(a) Overall Mesh (b) Inflation Layers

Figure 24: Volute Mesh

The default domain is set to rotating at -12000 Rpm, i.e. rotating clockwise, while the outlet passage is set to counter-rotating. Thus the outlet passage, or diffuser, is not moving. The arrows pointing outwards of the domain represents the mass flow boundary condition at the outlet, while the arrows at the inlet represents the total pressure boundary condition. As seen from figure 23, the outlet had to be extended. The reason for this is to avoid recirculating flow patterns at the outlet, since outlet boundary conditions only allows flow out of the domain [14].

9.2 Fluid Properties

The fluid which is to be used as propellant in the rocket engine is a mixture of approximately 75% ethanol and 25% water, and the relevant fluid properties for simulation can be seen in Ta

As seen in Table 4, the liquid is more than twice as viscous as water.

9.3 Full Simulation

Also for the full simulation, symmetry was utilized for the impeller, hence simulating only one passage. The volute was meshed using ANSYS Meshing, with an unstructured grid. The volute mesh can be seen in Figure 24a a and b, with a showing the overall mesh, and b showing the inflation layers placed at the volute walls. When conducting the full simulation, leakage was not taken into account, as this would have demanded much more computing power and time.

Simulation	Elements	Nodes
N_1	19 338	23 196
N_2	54 000	61 812
N_3	112 014	124 520
N_4	241 584	262 276
N_5	526 991	561 640

Table 5: Mesh Dependence

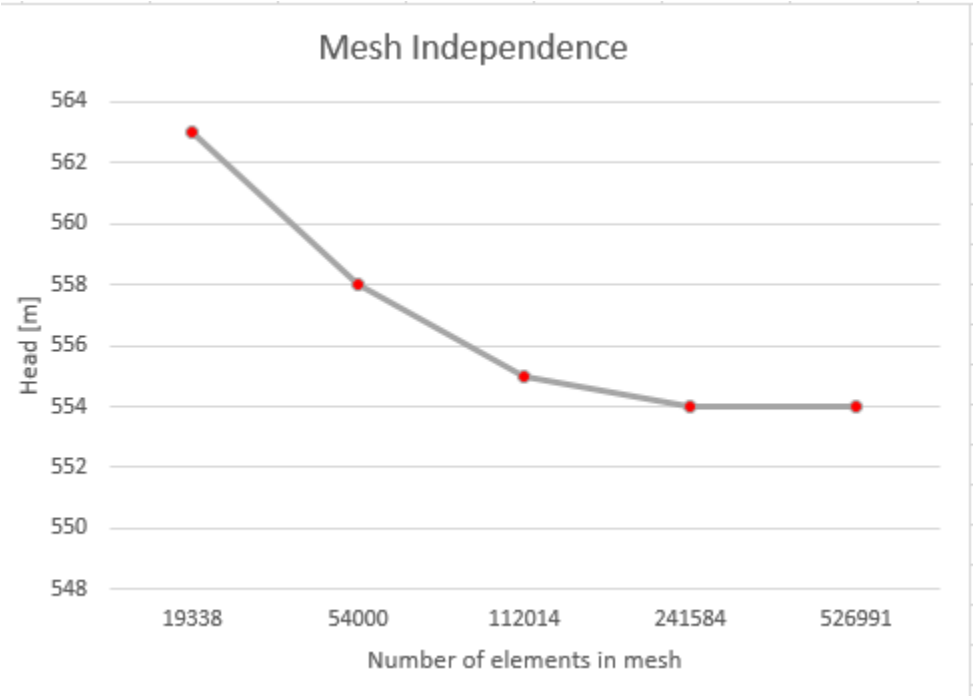

Figure 25: Head of Each Simulation

10 Numerical Results

10.1 Mesh Independence

In order to ensure that the solution is independent of the mesh, a mesh independence study has been performed. This is done by starting with a number of elements, N_1, and increasing the number of elements N_2,N_3,N_4 and N_5. until the solution does no longer change when refining the mesh further. The element and node count is for one blade passage, so if the the entire impeller was simulated, these numbers would have to be multiplied by 6. The mesh and node count for each simulation can be seen in table

The head, H as a function of N can be seen in Figure 25

As Figure 25 shows, the solution does no longer change when refining the mesh more than what is done in simulation N_4. It should be mentioned that the solution only changes about 1.5% from N_1 to N_5.

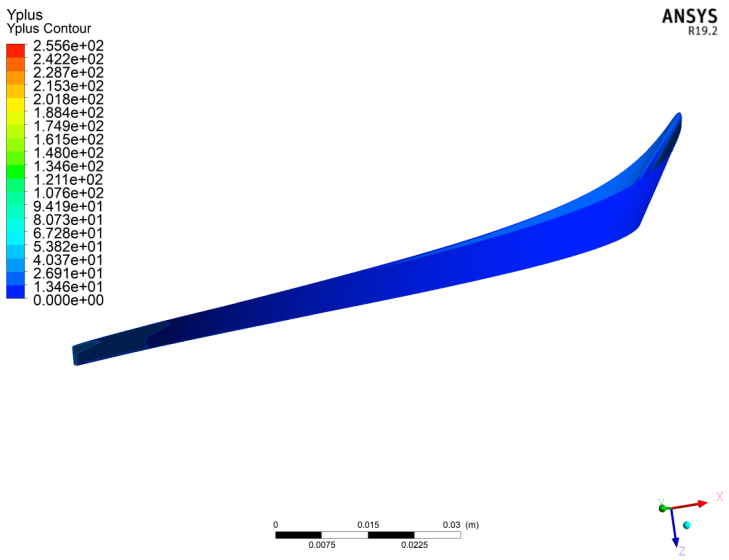

Figure 26: Y^+-values on pressure side of the blade

10.2 Y^+

As mentioned in section 8.2, there is no lower limit for Y^+ when using ANSYS CFX. The Y^+-values along the blade boundaries are shown in Figure 26 and 27 for the pressure and suction side respectively:

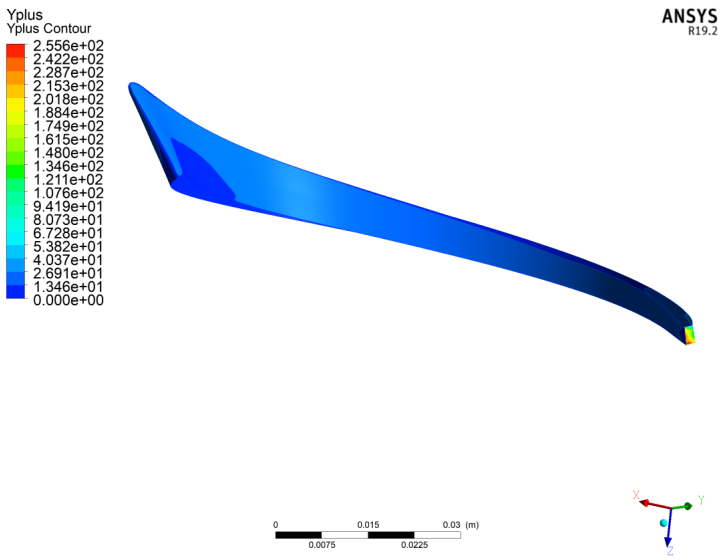

Figure 27: Y^+-values on suction side of the blade

Head	555 [m]
Efficiency	0.845
Shaft Power	110 096 [W]

Table 6: Boundary Conditions.

The value of Y^+ is around 11 on all blade boundaries except the trailing edge. Here the max value is 255, marked with red colour in Figure 27, which is still below the maximum allowed value for the $k-\epsilon$ turbulence model. Hence, the boundary has been resolved according to the criteria for this model. The Y^+-value is of great importance in this simulation due to the size of the pump, which causes friction to be the main source of hydraulic losses.

10.3 Overall Performance

The overall performance can be seen in Table 6:

10.3.1 Pressure

Figure 28, 29 and 30 shows the pressure distribution throughout the impeller for a radial span of 20%, 50% and 80%, where 0% is the hub, and 100% is the shroud. The lowest pressure can be seen at leading edge and is around 0.5 bar, which is well above the vapour pressure for the fluid, hence there should be no risk of cavitation. A low pressure point can also be located at the pressure side of the trailing edge. Due to the sharp edge, the flow will detach and create a recirculation zone at this point, and thereby create a pressure drop. The pressure gradually increases from 0.5 bar at the leading edge to around 35 bar at the trailing edge.

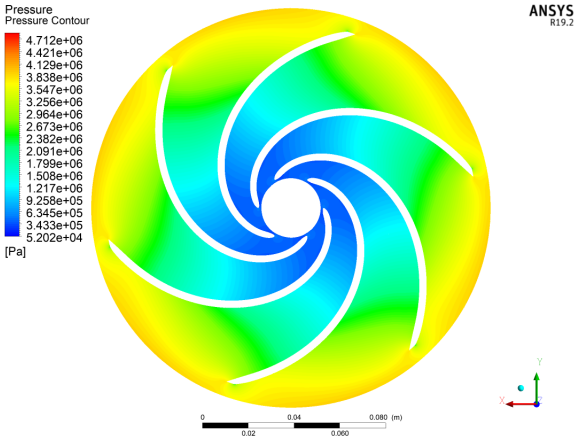

Figure 28: Pressure plot at 20% of the radial span

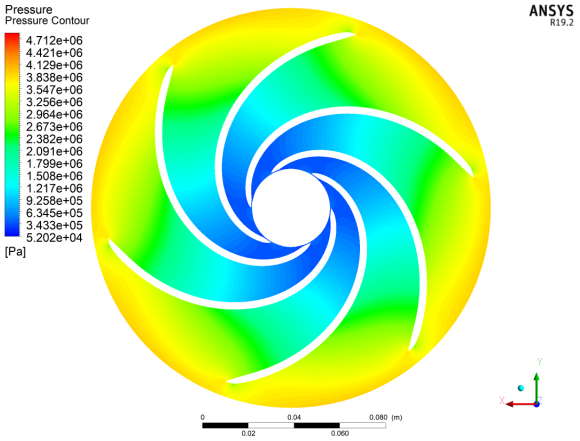

Figure 29: Pressure plot at 50% of the radial span

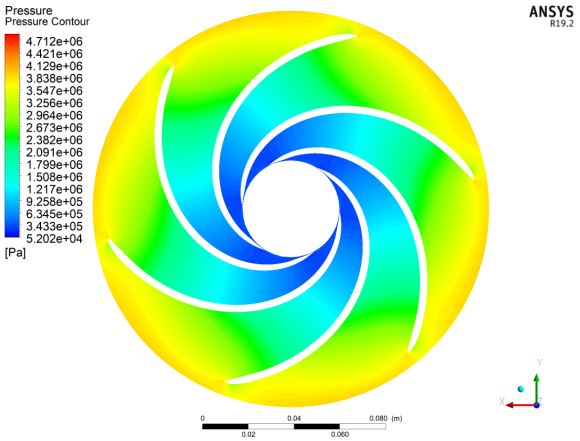

Figure 30: Pressure plot at 80% of the radial span

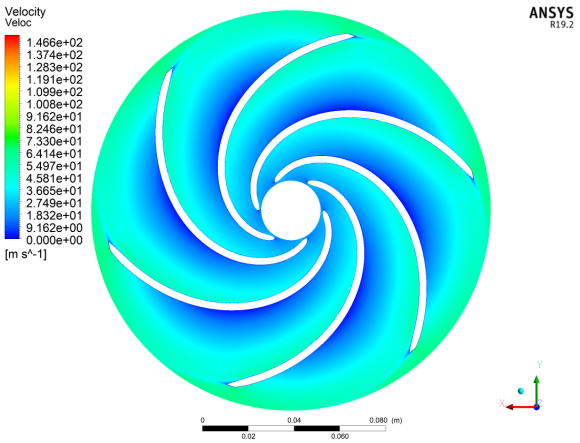

Figure 31: Velocity contour at 20% of the radial span

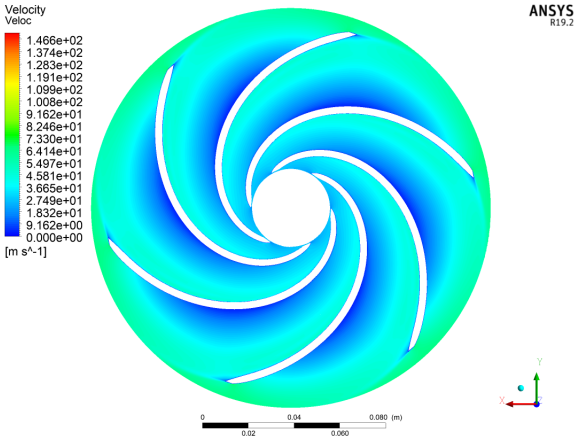

Figure 32: Velocity contour at 50% of the radial span

10.3.2 Velocity Contours

Figure 31, **??** and 33 shows the velocity contours at the same radial spans as for pressure. The lowest velocities can be seen at 20% of the span, where large areas of velocities below 3 m/s are present. These are areas where recirculating flows might occur. On the suction side the velocities are close to 40 m/s.

10.3.3 Surface Streamlines

Figure 34, 35 and 36 shows the surface streamlines. None of the spans show sign of recirculating flow patterns, and the flow stays attached throughout the impeller.

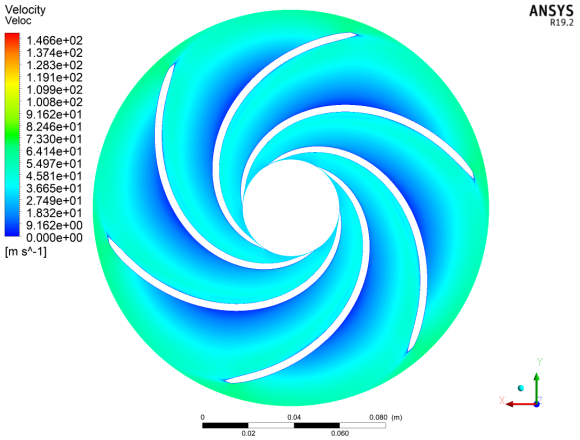

Figure 33: Velocity contour at 80% of the radial span

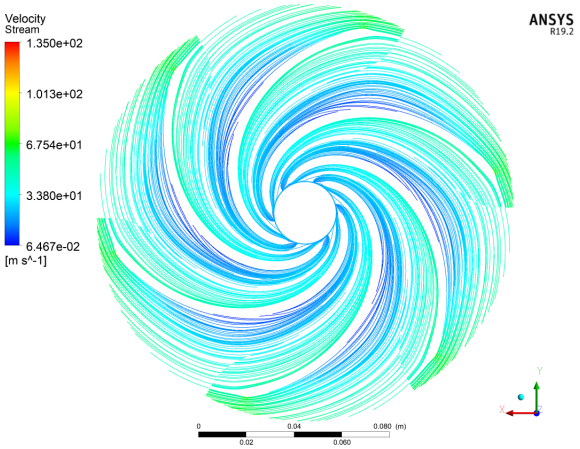

Figure 34: Surface streamlines at 20% of the radial span

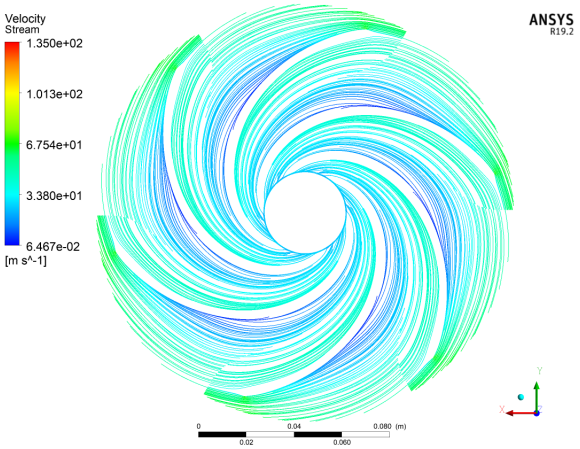

Figure 35: Surface streamlines at 50% of the radial span

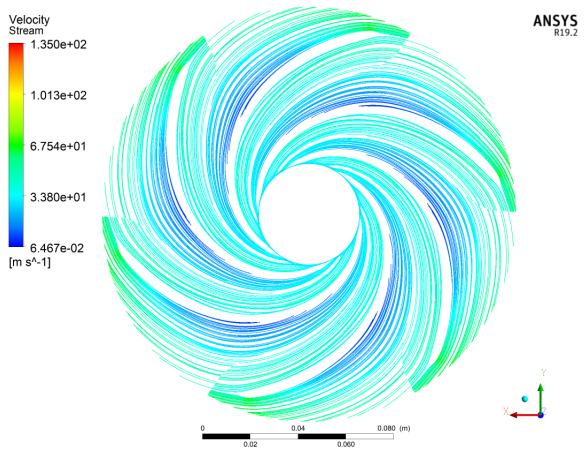

Figure 36: Surface streamlines at 80% of the radial span

11 Discussion

The results from the impeller analysis shows promising, although it is expected for any well designed impeller to reach hydraulic efficiencies above 90% when performing CFD-analysis, due to the fact that the surface of the impeller is smooth. Imperfections due to machining or casting quality is one of the main factors decreasing the hydraulic efficiencies in smaller pumps. Increasing the outlet height would lessen these losses, but the flow would most likely detach in the impeller, generating even greater losses. Near the outlet of the impeller, the boundary layers are relatively large. The fluid domain at this area consist of almost 30% boundary layer, and the flow nearly develops a laminar profile. As the friction factor increases with decreasing velocities, this is of course unfavourable.

The inlet diameter was chosen smaller than the one suggested by empirical data, which suggested an inlet diameter at 6.4 cm, due to the fact that the pressure at the leading edge dropped below vapor pressure when the diameter was set larger than 2.4 cm. The narrow inlet diameter would of course imply a further distance for the fluid to travel, leading to greater friction losses, but considering the damaging effects of cavitation, this was considered a better option. An alternative option would have been to design an inducer to increase the pressure at the pump inlet, and designed the inlet diameter as suggested by empirical data. This was however disregarded as the final design proved to be satisfactory.

The simulation of the entire pump did not reach a satisfying convergence criteria, and was chosen not to be presented in the result section. The criteria was set to 10^{-5} for the mean root residuals, but for the simulation these values never got below 10^{-3}. The two main reasons for this is assumed to be the element size difference between the outlet of the impeller and the inlet of the volute, and the low orthogonal quality of the volute mesh. The minimum recommended orthogonal quality is 0.1, while the volute mesh had a large number of elements below 0.002. A possible solution for improving the mesh is through ICEM meshing in ANSYS, but as time was a limiting factor this was not accomplished.

12 Conclusion and Further Work

A centrifugal pump for delivering high pressure fuel in a rocket engine has been designed. The impeller results has shown satisfactory with the design parameters in terms of head and power requirements. The calculated pressure difference from inlet to outlet achieved through CFD was roughly 46.5 bar, with an hydraulic efficiency of 84.5%. The relatively low efficiency is a result of large friction forces due to low clearance between the hub and shroud. The requirement of no cavitation was also fulfilled with a decreased inlet diameter.

The simulation of the pump in its entirety was not accomplished due to poor mesh quality and time limitation.

In order to determine the hydraulic performance of the entire pump, a full CFD-analysis must be performed. The mechanical design also have to be completed in order to determine the disk friction and leakage, which have major impact on the total efficiency. When this is completed, the pump has to be built and tested in the lab to determine the actual performance.

13 Bibliography

References

[1] J. F. Gülich, *Centrifugal Pumps*. Springer, 2nd edition, 2010.

[2] W.E Campbell, J. Farquhar. *Centrifugal Pumps for Rocket Engines*, NERVA Rocket Operations, Aerojet Nuclear Systems Company.

[3] A. J. Stepanoff. *Centrifugal and Axial Flow Pumps*. 2nd edition. Wiley, 1957.

[4] http://pumps.org/Pump_Fundamentals/Pump_Terms_and_Definitions.aspx

[5] Z. Wei, P.H. Finstad, G. Olimstad, E. Walseth, M. Eltvik, *High Pressure Hydraulic Machinery*, NTNU, December 2009.

[6] I. Karassik, *Pump Handbook*, 2nd edition. McGraw - Hill, New York, 1995.

[7] D. H. Huang, D. K. Huzel, *Design of Liquid Propellant Rocket Engines*, NASA, Washington, DC, 1971.

[8] L. Tan, *Influence of Blade Wrap Angle on Centrifugal Pump Performance by Numerical and Experimental Study*, Chinese Journal of Mechanical Engineering 27(1):171-177, January 2014

[9] ANSYS. *CFX-Solver Modeling Guide 14.0*, 2011.

[10] https://www.sharcnet.ca/Software/Ansys/17.0/en-us/help/cfx_intr/i1301908.html

[11] https://www.pumpsandsystems.com/function-volute

[12] F. J. Wiesner, *A Review of Slip Factors for Centrifugal Impellers*, J.Eng. Power 89(4), 558-566, October 1967.

[13] R. Tao, R. Xiao, *Influence of Blade Leading-Edge Shape on Cavitation in a Centrifugal Pump Impeller*, Energies, MDPI, Open Acces Journal, vol.11(10), pages 1-16, September 2018

[14] https://www.sharcnet.ca/Software/Ansys/16.2.3/en-us/help/cfx_mod/i5500692.html

[15] S. L. Dixon, C. A. Hall, *Fluid Mechanics and Thermodynamics of Turbomachinery*,7nth edition, Elsevier Inc. 2014

[16] Huzel, D. K., Huang, D. H., Arbit, H.*Modern engineering for design of liquid-propellant rocket engines* . Washington, D.C: American Institute of Aeronautics and Astronautics, Vol. 147, 1992.

[17] X. Han et al. *Impeller Optimized Design of the Centrifugal Pump: A Numerical and Experimental Investigation*, Energies 11(6):1444, June 2018

[18] M. Asuaje et al, *Numerical Modelization of the Flow in Centrifugal Pump: Volute Influence in Velocity and Pressure Fields*, International Journal of Rotating Machinery 3(3), January 2005

[19] B. Neumann, *The interaction between geometry and performance of a centrifugal pump*, 1 edition, Wiley, 2005.

[20] J. Tuzson, *Centrifugal Pump Design* . Wiley, 2000.

[21] H. Brekke, *Pumper og Turbiner*, Vannkraftlaboratoriet, NTNU, 2003

[22] S. S. Foslie, *Design of centrifugal pump for produced water*, Project Thesis, Norwegian University of Science and Technology, 2013.

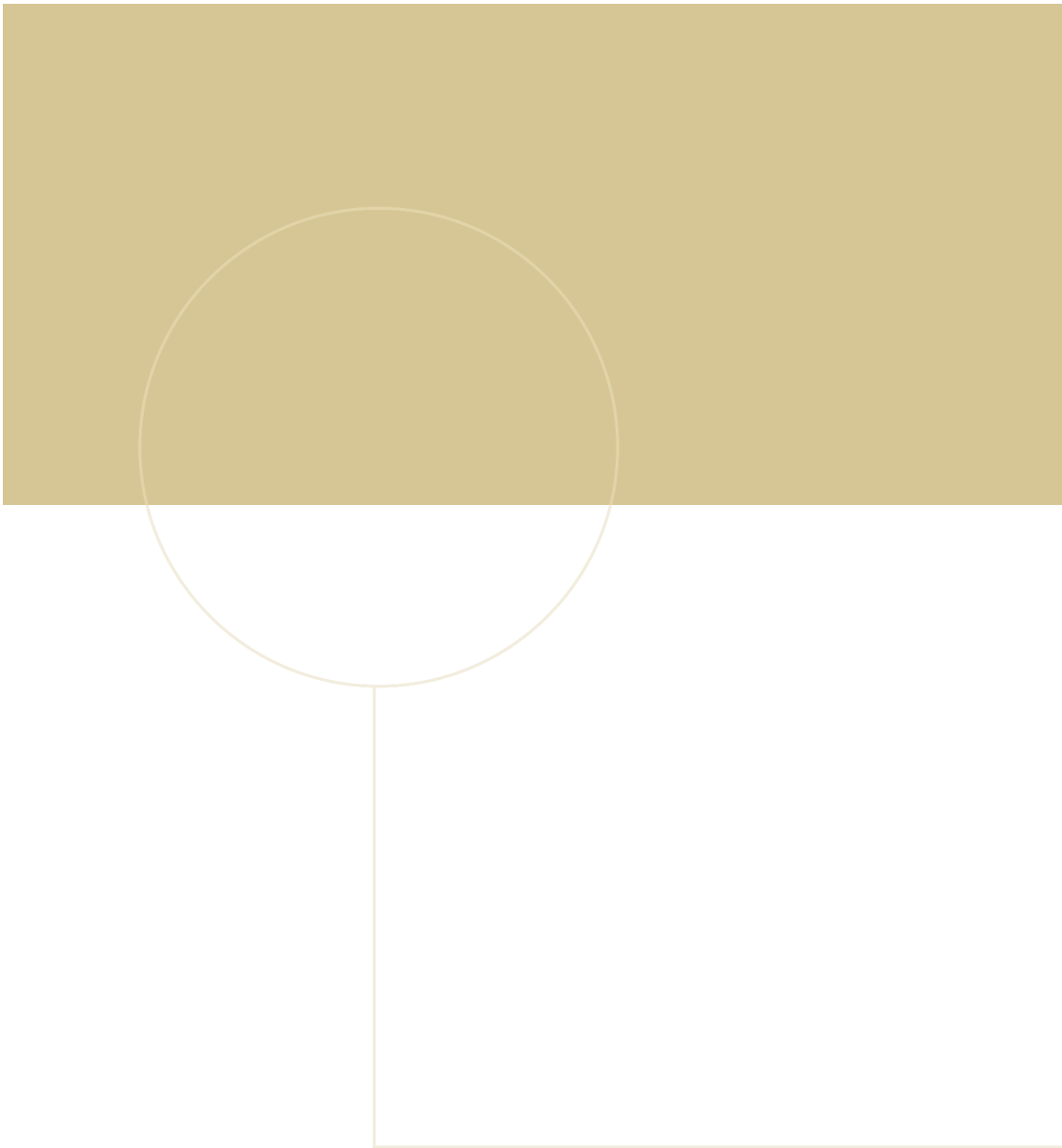

NTNU

Kunnskap for en bedre verden